Original Study **Open Access**

L. Koene*, N.V.H. Schouten, R. Savelsberg

Feasibility of kinetic orbital bombardment

DOI 10.2478/jms-2024-0001
Received: January 31, 2023; Accepted: September 13, 2023

Abstract: In this paper, the possible impact effects of orbital bombardment systems and their feasibility are studied. These effects are the projectile penetration into concrete and steel targets and seismic effects. The equations of motion for the re-entry of a projectile and the penetration were solved numerically. The projectile penetration is modelled using the Alekseevskii–Tate model. By varying the altitude (h), projectile length (L), manoeuvre velocity (ΔV) and the target properties, the flight time (t), earthquake magnitude (M) and penetration depth (P) are calculated. The calculations show that the impact of a tungsten alloy rod with a length of 8 m and a 0.4 m diameter results in an earthquake with a seismic magnitude of only 2.5 on the Richter scale. For concrete, the optimal result is obtained for a projectile with a length of 0.56 m. It penetrates 1.79 m with a minimal ΔV trajectory. These results show that a kinetic orbital bombardment system is not feasible without major technological developments, the impact angle being a bottleneck of the concept. Moreover, one has to accept very high costs. Without any means to change the attitude of the projectile, using ICBMs or bombers shows a better penetration performance than re-entry.

Keywords: orbital bombardment, Rods from God, Hohmann transfer, atmospheric re-entry, Tate–Alekseevskii penetration model

Highlights:

- Weapons in orbit may provide a strategic advantage. However, they are restricted by international space laws.
- Impact angle of the projectile is a bottleneck for kinetic orbital bombardment.
- Larger impact angles can be achieved, but at the expense of a larger mass-to-orbit.
- A hypersonic drag device may be used to optimise the impact angle and thus improve the system.
- Alternative projectile delivery methods (Bomber, Intercontinental Ballistic Missile (ICBM)) show better performance for both steel and concrete targets.
- Essentially, only penetration phenomena matter because the seismic effects are not significant. Therefore, orbital bombardment systems don't even resemble weapons of mass destruction (WMD).
- Given their limited effect, destroying a particular target requires a guidance and flight control system, which, given the high velocities, may not be feasible.

1 Introduction

During the Cold War, the United States investigated the possibility of using the space domain for weapons, by having a satellite in orbit carrying long tungsten rods, which could deorbit and impact the Earth with a high velocity, thereby causing damage. The United States Air Force even tested orbital bombardment, but little information can be found about those tests. In literature, this concept is often considered to be a superweapon, capable of striking anywhere in the world at short notice, and as a suitable alternative to small nuclear 'bunker busters'. However, this claim is not supported by scientific research.

At present, the military uses of the space domain are primarily communications and Intelligence, Surveillance and Reconnaissance (ISR). However, in this work, the concept of orbital bombardment and its present feasibility will be investigated. When studying this concept, it is good to bear in mind that laws also apply to space. In 1966, at the peak of the Space Race, the Soviet Union and the United States agreed on an Outer Space Treaty, by the United Nations (UN), which states the following (UN Outer Space Treaty of 1966; Article IV 1966):

> *'States Parties to the Treaty undertake not to place in orbit around the Earth any objects carrying nuclear weapons or any other kinds of weapons of mass destruction, install weapons on celestial bodies, or station weapons in outer space in any other manner.'*

***Corresponding author: L. Koene,** Faculty of Military Sciences, Netherlands Defense Academy, Den Helder, Noord-Holland, Netherlands, E-mails: lkoene@dds.nl, l.koene@mindef.nl
N.V.H. Schouten and R. Savelsberg, Faculty of Military Sciences, Netherlands Defense Academy, Den Helder, Noord-Holland, Netherlands

Evidently, this treaty created boundary conditions for weapons that are allowed in orbit. Incidentally, placing nuclear warheads in ballistic missiles does not constitute a violation, because they fly suborbital trajectories instead of orbits. A kinetic orbital bombardment system consists of a satellite in orbit around the Earth with a bus of multiple heavy metal (tungsten or depleted uranium) rods. These rods can be deorbited, and their kinetic energy upon impact can destroy targets on Earth (Watts 2005). The great advantage of such a weapon system is the rapid response time and, with a suitable constellation, every target on Earth can be hit. Another advantage is that it is not a 'doomsday weapon', the use of which would have catastrophic effects, and as such it would not violate the Outer Space Treaty. This weapon system can be used in both small conflicts and larger conflicts, because the projectile does not have an explosive warhead, and thus little collateral damage is expected from these weapons. The US Air Force explored this idea from 1978 to 1988, including at least one flight test from Vandenberg Air Force Base (AFB) to Kwajalein Atoll, using a suborbital trajectory (Watts 2005). Very few technical details are known, but the program was reportedly terminated because 'Air Force fighter generals were not interested in a non-nuclear global weapon' (Watts 2005).

However, the Air Force's 2003 Transformation Flight Plan included plans for orbiting weapons, including hypervelocity rod bundles, called 'Rods from God'. According to Johnson-Freese (2017), the idea was not new or even original. The science fiction writer Pournelle (1974) conceived it while working at Boeing in the 1950s. He called it 'Thor'. Pournelle (1974) was well-aware of the (strategic) importance of orbit around Earth, which is reflected by a conversation with the well-known science fiction writer Robert A. Heinlein (Pournelle 1974):

> *"Aha," I said. "I see your problem. "If you can get a ship into orbit you're halfway to the moon." "No," Bob [Heinlein] said. "If you can get your ship into orbit, you're halfway to anywhere." He was very nearly right.*

As far as is known, *Rods from God* remained only a concept, see e.g. Johnson-Freese (2017). However, this concept inspired science fiction writers. In the novel Quantico (2005) by Bear (2005) steel telephone poles called 'Rods from God' guided by lasers are used to take out trucks that carried deadly cargo. In the military science fiction movie *G.I. Joe: Retaliation* (2013) the villain created 'Project Zeus' that consisted of seven kinetic orbital bombardment systems that were depicted as weapons of mass destruction (WMD), even more effective than nuclear warheads. In addition, the idea that orbital bombardment is a WMD is spread in popular scientific and military press, see e.g. Larson (2020) and Stilwell (2020). None of this literature provides a quantitative description of how such a kinetic orbital bombardment system could work.

In this orienting work on kinetic orbital bombardment, we have studied the most essential features of both the projectile trajectory from orbit and the expected target penetration, including the seismic effects. For this reason, it was inevitable to make simplifications. For instance, the impact model is a 1D semi-hydrodynamic model. It is used to calculate the penetration depth. However, the overall model includes oblique impact and projectile ricochet to allow for a realistic evaluation of the concept. Seismic effects have been estimated to demonstrate that these are much smaller than for a weapon of mass destruction, and they are thus restricted to the direct vicinity of the target.

The structure of this paper is as follows. First, the relevant theory is discussed, i.e. for calculating the flight trajectories, target penetration, seismic effects of kinetic impact, and material properties of the targets and projectiles. After this theory is discussed, the results from the study are presented. The flight trajectories of the projectiles are calculated using a computer. To calculate the projectile penetration, the Tate-Alekseevskii (TA) model is simulated. Finally, flight trajectories and target penetration simulations are combined, including oblique impacts and ricochets. This is followed by a discussion and conclusions.

2 Kinetic orbital bombardment modelling

The present exploratory research aims to better understand the capabilities of the space weapon by qualitatively and quantitatively mapping the influence of different parameters involved. This is done using computer simulations. The flight parameters, i.e. altitude, projectile length (L) and manoeuvre velocity (ΔV), determine the flight trajectory with the other initial conditions. The output of the flight simulation, being impact velocity v_0 and impact angle γ, are the input for the impact simulation. The outputs, the dependent variables, are the penetration depth P and the seismic magnitude M, as well as the flight time. The influence of the independent or input variables is studied by varying them in the simulations and analysing the results. Little knowledge is presented

in literature about any of the aforementioned variables. Only Watts (2005) and Elbasheer (2014) provide details of the projectile's length and possible targets. Watts (2005) states that 4″–5″ tungsten projectiles can be used for soft areas such as airfields, and longer 1–2 m projectiles can be used for deep underground facilities, missile silos, tall buildings and low, vulnerable buildings. Elbasheer (2014) describes a larger, 6.1 m tungsten projectile and the same type of targets.

Material properties are another vital aspect of this study, as a projectile would penetrate deeper into a softer material than in a harder material, e.g. concrete instead of armour. These properties are used in the penetration modelling. As stated above, the primary targets are urban structures such as airfields, tall buildings and missile silos. Most such structures are made of concrete or steel. Hence, those will be the main material used for this study. In the study, it is assumed that a perpendicular impact with respect to the Earth's surface is optimal for penetrating the target.

2.1 Projectile flight model

To calculate a trajectory, the initial conditions must be determined first. They serve as a starting point for the re-entry simulation. The focus of this study is orbital re-entry, where a satellite in orbit around Earth manoeuvres the projectile so that it falls towards Earth's surface. This scenario is shown in Figure 1. In order for the projectile to hit a target on the Earth's surface, it needs to manoeuvre and enter the atmosphere and go through orbital re-entry. The orbital velocity, V_{orbit}, is given by

$$V_{\text{orbit}} = \sqrt{\frac{\mu_{\oplus}}{R}}, \tag{1}$$

with $\mu_{\oplus} = M_{\oplus}G$, where G and $M_{\oplus}$ are the gravitational constant and the mass of the Earth, respectively, and R is the distance to the centre of the Earth:

$$R = R_{\oplus} + h, \tag{2}$$

where $R_{\oplus}$ represents the radius of the Earth and h the altitude. Note that the orbital velocity is not a function of vehicle mass, only of the altitude. To change altitude, to ultimately strike the surface of the earth, the velocity of the vehicle has to change. That velocity change is called ΔV, see e.g. Curtis (2005) and Wiesel (2010). In the most energy-efficient manoeuvres, so-called Hohmann transfers, the ΔV is parallel to the flight path. In case ΔV is applied to

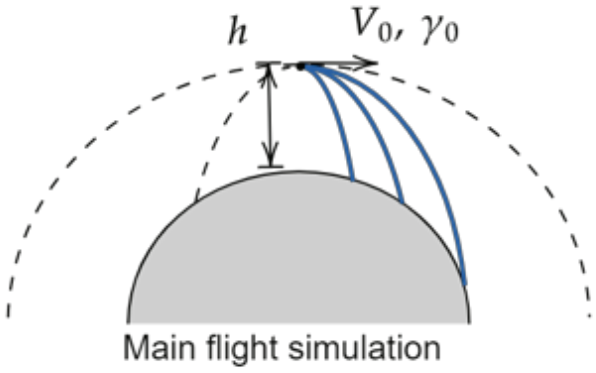

Fig. 1: Initial conditions for the re-entry simulation.

increases the velocity, the altitude on the opposite side increases to a more elevated orbit. To deorbit a projectile, ΔV reduces the velocity, which causes the opposite side of the orbit to lower until the atmospheric drag decelerates the projectile further and it is captured. The amount of velocity change determines the steepness of the re-entry trajectory.

In order to induce this change in velocity the projectile needs to be equipped with a retro-rocket that thrusts the projectile in the opposite direction of the flight direction. This manoeuvre burns propellant, which has to be carried by the satellite. To estimate the amount of propellant necessary for the manoeuvre, the Tsiolkovsky rocket equation is used:

$$\Delta V = I_{\text{sp}} g_0 \ln\left(\frac{m_{\text{i}}}{m_{\text{f}}}\right) \tag{3}$$

where I_{sp} is the specific impulse of the propellant and g_0 is the gravitational acceleration at the surface of Earth. The mass m_{i} is the initial mass, prior to the burn, i.e. the mass of the rod and the rocket motor, including the propellant. The mass m_{f} is the final mass, i.e. the mass of the rod and the rocket motor after the propellant has been burned.

Figure 2 displays a diagram of the re-entering projectile, with orange arrows representing the velocity vector and blue arrows portraying the forces acting on the projectile.

The re-entry model used includes aerodynamic drag. Once the initial conditions are acquired, they are put into the re-entry simulation, which is bound by several assumptions:

- The scenario is two-dimensional.
- The Earth is modelled as a perfect sphere with gravity pointing down to the centre of the coordinate system; gravity is altitude dependent.

- Earth rotation is not included.
- The effect of wind is neglected.
- The atmosphere is modelled using the International Standard Atmosphere, see e.g. Anderson (2016).
- The rod experiences aerodynamic drag, $F_D = \frac{1}{2}\rho V^2 S C_D$, where ρ is the air density, V is velocity, S is the cross-sectional area of the projectile and C_D is the drag coefficient. The drag coefficient will further be elaborated in Section 2.1.1.
- The projectile is symmetric and the angle of attack of the projectile is effectively zero, and thus it generates no lift.

The latter point can be understood as follows. To keep the projectile stable during flight, it would have to be fin-stabilised. Tailfins ensure that, if the projectile were to gain an angle of attack, the aerodynamic force moment on the tail counteracts this motion, thus stabilising its flight and limiting the angle of attack. Furthermore, the projectile is assumed to be unguided during the atmospheric flight.

When the projectile travels at a hypersonic velocity, through the atmosphere, the air molecules ionise and a plasma forms around the projectile. This plasma blocks Electromagnetic (EM)-transmission (Bond 1958), which is essential for communication. This means that no external input can be given to navigate the projectile. Another way to guide the projectile to its target is to use a seeker head, but building a seeker capable of withstanding the high temperature may not be feasible. Finally, flight control would be problematic, since, if the angle of attack were to become too large, the force moment on the projectile might cause it to break up in flight.

The equations of motion for the subsequent suborbital trajectory are given by Hankey (1988).

$$\dot{R} = V\sin(\gamma) \tag{4a}$$

$$\dot{V} = -\frac{\mu_\oplus}{R^2}\sin(\gamma) - \frac{\rho V^2 S C_D}{2m} \tag{4b}$$

$$\dot{\theta} = \frac{V}{R}\cos(\gamma) \tag{4c}$$

$$\dot{\gamma} = \frac{V}{R^2}\cos(\gamma) - \frac{\mu_\oplus}{VR^2}\cos(\gamma) \tag{4d}$$

The parameters m and y are the projectile mass and the flight path angle (see Figure 2), respectively. The parameters $\dot{R}$, $\dot{V}$, $\dot{\theta}$ and $\dot{\gamma}$ are time derivatives, and conform to Newton's notation. By numerically integrating these equations with respect to time, the altitude, velocity, pitch and distance can be calculated as a function of time. This is done using MATLAB SimuLink®.

2.1.1 Aerodynamic properties of the projectile

The drag coefficient of the projectile depends on its shape and the Mach number. As no information about actual orbital projectiles is available, we have to make some assumptions about the projectile. Elbasheer (2014) proposed a length of 6.1 m and a diameter of 0.3 m with a length over diameter *(L/D)* of 20. In this paper, we consider a range of different projectiles, each essentially cylindrical and with the same *L/D* ratio with lengths between 0.1 m and 6.1 m. For a tungsten alloy projectile, this corresponds to a mass between about 0.03 kg and 7,600 kg.

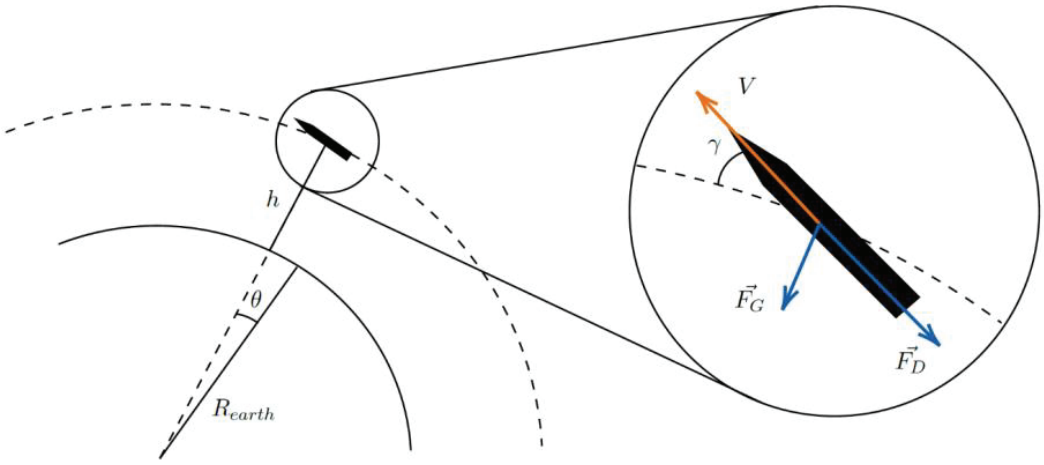

Fig. 2: Diagram of the re-entering projectile.

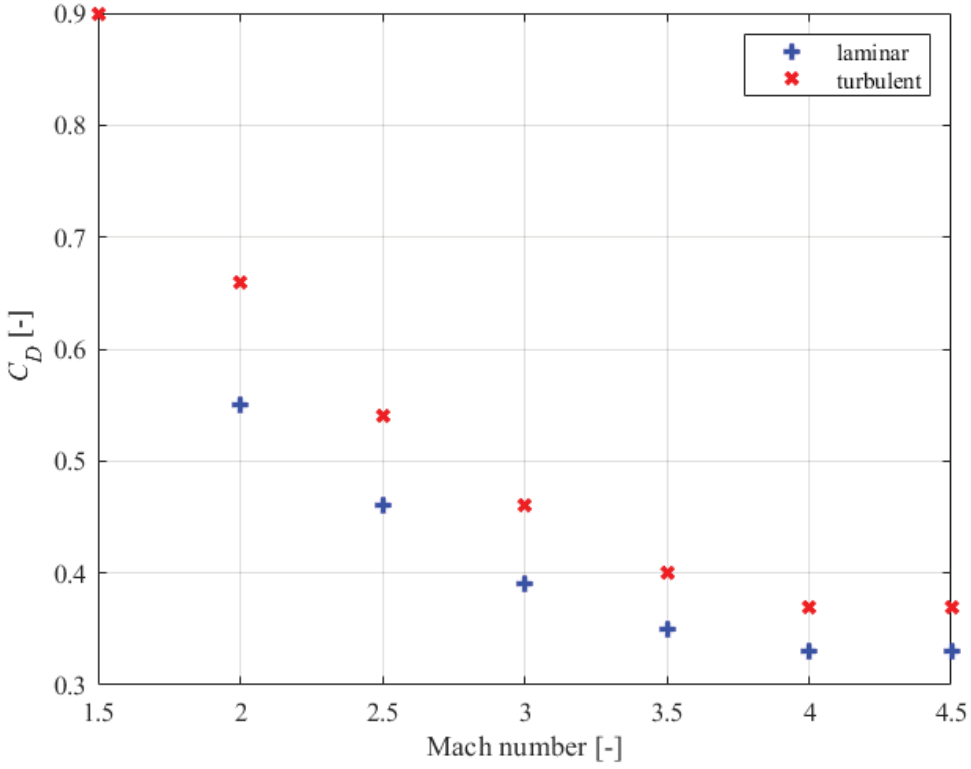

Fig. 3: Drag coefficient (C_D) vs. Mach number for the XM110 projectile for both laminar and turbulent flow. This graph is based on data collected by Braun (1973).

Assuming the projectile has a flechette-like shape, a close resemblance can be found in the XM110 projectile with an L/D of 23. Braun (1973) established a database for small arms aerodynamics, which includes aerodynamic data for a XM110 projectile for both laminar and turbulent flow (see Figure 3). Owing to the high velocity of the projectile, it is easy to gravitate towards assuming a fully turbulent flow. The Reynolds number helps to predict the type of flow. The Reynolds number is the ratio of internal forces and viscous forces: a high Reynolds number is associated with turbulent flow and a lower Reynolds number with a laminar flow. The Reynolds number is defined as:

$$\mathrm{Re} = \frac{\rho V L}{\mu} \tag{5}$$

where ρ represents the density of the fluid, V is the fluid velocity, L is the characteristic length and μ is the dynamic viscosity, see e.g. Hibbeler (2020). It depends on the temperature of the fluid and is defined as (Chapman and Cowling 1970; Zheng et al. 2016):

$$\mu = \left(\frac{T}{288.15}\right)^{3/2} \frac{288.15 + c}{T + c} \mu_{288.15} \tag{6}$$

where T is the fluid temperature, c is a fluid specific parameter and $\mu_{288.15}$ is the viscosity at a temperature of 288.15 K. Eq. (6) is known as Sutherland's formula and c is the so-called Sutherland constant (Chapman and Cowling 1970). For air c = 110.4 K and $\mu_{288.15} = 1.822 \times 10^5$ Pa/s, the critical Reynolds number indicates a fluid transition from a laminar to a turbulent flow. For a viscous flow over an external surface the critical Reynolds number is $\mathrm{Re}_{cr} = 5 \times 10^5$ (see e.g. Hibbeler 2020). In the simulations, the flow is turbulent above Re_{cr} and laminar below Re_{cr}. To model the behaviour, the temperature is calculated using the international standard atmosphere (Anderson 2016). The simulation uses a switch case where, depending on the Reynolds number, it takes data either from the turbulent flow graph or from the laminar flow graph.

By simulating two trajectories, with one assuming fully turbulent flow and the other considering both types of flow, the difference can be observed. To best visualise the effect, a trajectory with a long flight path through the atmosphere is chosen. Thus, the projectile experiences the longest time under the influence of aerodynamic drag. Normally the flow transitions at the critical velocity. This transition means that there is a grey area where it could be either turbulent or laminar. Furthermore, an initial altitude of 400 km and a projectile with L = 8 m are chosen.

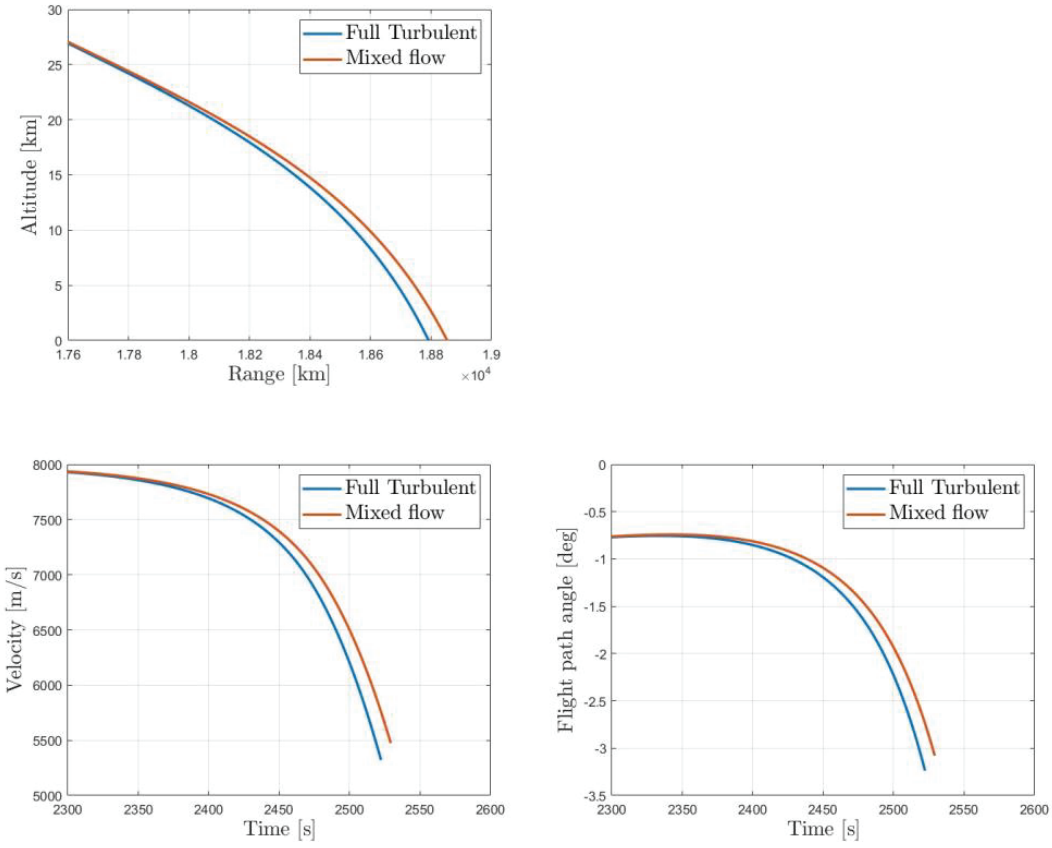

Fig. 4: Flight trajectory (a), velocity (b) and path angle (c) to test the influence of the Reynolds number.

The resulting trajectory, flight velocity and pitch can be seen in Figures 4a, 4b and 4c, respectively. As all three figures show, a minor difference can be seen for the different methods. The impact velocity deviates 2.72%, the pitch deviates 4.70%, the flight time deviates 0.28% and the range deviates 0.32%. This is included in the model, although the effect is small.

2.2 Projectile penetration model

To describe the projectile penetration into concrete and steel a semi-hydrodynamic model was chosen, i.e. the 1D-model of Tate and Alekseevksii. Of course, this 1D-model is less advanced than, for instance, models based on cavity expansion theory. However, it is a classical model that ought to be capable of adequately estimating the penetration depth of long rod projectiles in steel and concrete. The characteristic equation of Tate and Alekseevskii (see e.g. Alekseevskii 1966; Tate 1969; Hohler and Stilp 1990; Walker 2021) is a modified Bernoulli equation:

$$\frac{1}{2}\rho_p\left(v-u\right)^2+Y_p=\frac{1}{2}\rho_t u^2+R_t, \tag{7a}$$

where u is the penetrating velocity and v is the tail velocity of the projectile, and R_t and Y_p are, respectively, the dynamic penetration strengths of the target and the projectile. Eq. (7a) determines the penetration velocity u. This velocity can be explicitly determined because all parameters in this equation are known. In their model, Tate and Alekseevksii introduce a finite projectile length. During penetration the projectile is eroding. The equation for the deceleration of the projectile is:

$$\frac{\mathrm{d}v}{\mathrm{d}t}=-\frac{Y_p}{\rho_p L}, \tag{7b}$$

where $L(t)$ is the time dependent projectile length. The rate of change of the projectile length is given by:

$$\frac{\mathrm{d}L}{\mathrm{d}t}=-\left(v-u\right) \tag{7c}$$

Eqs (7a–c) are representative of the Tate and Alekseevksii model. These equations are integrated to obtain the penetration depth (P) and length (L) of the projectile as a function of time. The different penetration mechanisms of the Tate–Alekseevskii model are illustrated in Figure 5.

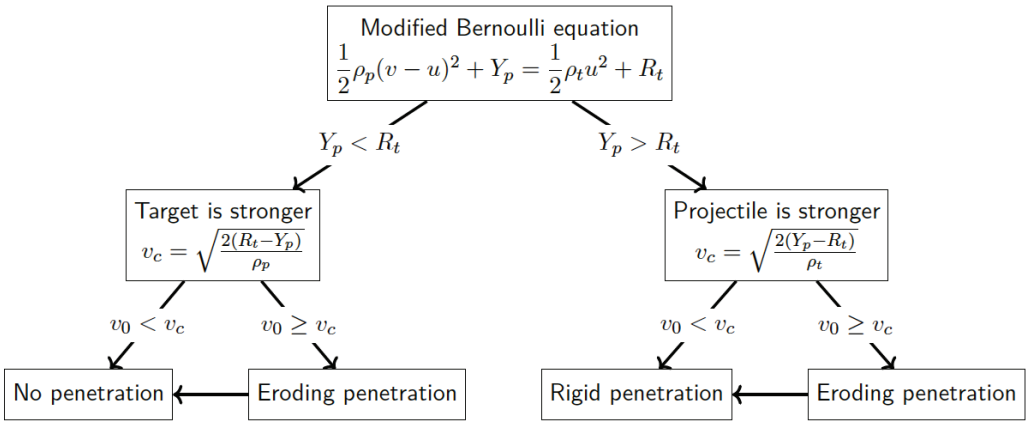

Fig. 5: Penetration mechanisms.

Evidently, the Tate–Alekseevskii model has limitations, for projectile impacts are 3D-phenomena. However, the penetration depth is for our purpose the most important parameter, and it can be described using the 1D-model. Moreover, the (finite) speed of sound in the material is not considered, see e.g. Walker (2021). The longitudinal speed of sound in metals is typically 5–6 km/s. As long as the projectile velocity is smaller than the speed of sound in the material, the effect can be considered to be negligible. For further limitations of the model, see e.g. Bavdekar et al. (2017, 2019).

2.2.1 Penetration model parameters

As said, material properties are a vital aspect of this study, as a projectile penetrates deeper into softer materials. The primary targets we consider are urban structures such as airfields, tall buildings and missile silos. Most such structures are made of concrete or steel. Hence, it is on these materials that this study will be focused. Table 1 shows different materials with their respective density (ρ_t) and unconfined compressive strength (f'_c). As seen in Table 1, geological materials are comparable with concrete because the unconfined compressive strength is in the same range.

For the impact simulations, the upper and lower bounds of the concrete properties are used. This gives the best indication for the minimum and maximum expected values for penetration depth. Not only are the properties of the target material important but also those of the projectile. The tungsten alloy rod has a density of ρ_p = 17,000 kg/m³ and a dynamic penetration strength of Y_p = 1.93 GPa (Tate 1986). An overview of the properties used in the simulations is provided in Table 2.

Tab. 1: Overview of relevant material properties.

Material	ρ_t [kg/m³]	f'_c [MPa]	R_t [GPa]
7 ksi Concrete [HJC]	2,440	48	-
SAC5 Concrete [N et al.]	2,299	37.9	-
WSMR-5 3/4 Concrete [SYG]	2,299	44.8	-
3.7 ksi Concrete [SYG]	1,990	25.5	-
Concrete [VLK]	2,300	51	-
Limestone [VLK] [WHP]	2,300–2,320	58–63	-
Sandstone [B et al.]	2,000–2,040	16–30	-
Steel [T]	7,850	-	3.45–5.18

Data sources are – for concrete: Butler, Nielsen, Dropek & Butters (1977); Holmquist, Johnson & Cook (1993); Warren, Hanchak & Poormon (2004); Noble, Kokko, Darnell, Dunn, Hagler & Leininger (2005); Stokes, Yarrington & Glenn (2005); Vahedi, Latifi & Khosravi (2008); and for steel: Tate (1986).
This table is inspired by the work of Flis (2016).

Tab. 2: Overview of material properties with dynamic penetration parameters.

Material	$\rho_t \left[\frac{\text{kg}}{\text{m}^3}\right]$	f'_c [MPa]	R_t [MPa]	Y_p [MPa]
Concrete (lower boundary) [SYG]	1,990	25.5	362	-
Concrete (upper boundary) [VLK]	2,300	51	495	-
Steel (lower boundary) [T]	7,850	-	3,450	-
Steel (upper boundary) [T]	7,850	-	5,180	-
Tungsten alloy [T]	17,000	-	-	1,930

Sources are given in the caption of Table 1.

To calculate the dynamic strength of concrete from the unconfined compressive strength, f'_c, the equation of Frew et al. (1998) was adopted:

$$R_t = f'_c S = f'_c\, 82.6 \left(\frac{f'_c}{10^6\ \text{Pa}}\right)^{-0.544} \tag{8}$$

So, to calculate dynamic strength, only a value of the compressive strength is necessary. The equation of Frew et al. (1998) is based on experimental data and valid for concrete with unconfined compressive strengths between 13.5 MPa and 97 MPa.

Granular materials such as soil or sand are not treated in this paper. These materials are also characterised by their grain size and have a very low target strength. Of course, penetration depths for long rods are expected to be higher than for both concrete and steel.

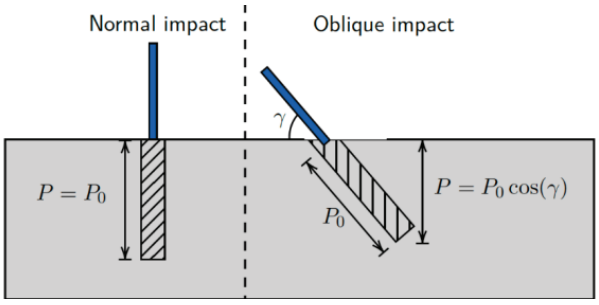

Fig. 6: Schematic of normal and oblique impacts. The blue bar represents the projectile and the dashed bar represents the impact cavity.

2.3 Oblique impact and ricochet

For realistic projectile impact simulations, both oblique impact and the possibility of ricochet have to be considered. First, we will treat ricochet. When the impact angle is too high with respect to the normal of the surface, the projectile skips off the surface. This is called ricochet. It is a complex projectile target interaction, but Tate (1979) developed a simplified model to calculate the critical ricochet angle β_{crit}. The projectile will ricochet if the impact angle is larger than the critical ricochet angle. The equation is as follows:

$$\tan^3(\beta) > \frac{2}{3}\frac{\rho_p v_0^2}{Y_p}\left(\frac{L^2+D^2}{LD}\right)\left(1+\sqrt{\frac{\rho_p}{\rho_t}}\right) \tag{9}$$

where β is the angle relative to the normal, ρ_p and ρ_t are the mass densities of the projectile and target, respectively, v_0 is the impact velocity, Y_p is the dynamic penetration strength, and L and D are the length and diameter of the projectile, respectively.

Penetration models, such as the TA-model, implicitly assume perpendicular impact. However, usually, the projectile will hit the target with an oblique impact angle. Since the velocity vector is in the same direction as the body axis of the projectile, the penetration depth can be calculated by simply correcting for the impact angle:

$$P = P_0 \cos\gamma = P_0 \sin\beta \tag{10}$$

where P is the penetration depth, P_0 is the penetration depth if the projectile would have impacted normal to the surface, and is the impact angle, as visualised in Figure 6. Note that y is the angle with respect to the surface, while $\beta = 90° - y$ is, as said, the angle relative to the normal.

2.4 Seismic effect of kinetic impact

When a rod impacts the ground, a small fraction of the kinetic energy is transferred into seismic energy. This fraction is known as the seismic efficiency k ($E_{seism} = k E_k$). If the seismic efficiency is known, an estimation can be made on the seismic effects by converting seismic energy to the Richter scale (Gutenberg and Richter 1955):

$$M = \frac{2}{3}\left(\log\left(E_{seism}\right) - 4.8\right) \tag{11}$$

where M is the earthquake magnitude according to the Richter scale. Güldemeister and Wünnemann (2017) conducted a quantitative analysis of impact-induced signals using numerical modelling. High velocity impacts were tested of spherical steel and iron meteorites into various materials. As a result of these tests, numerous seismic efficiencies were obtained for different target materials ranging between 1.37×10^{-4} (for 100% saturated sandstone) and 3.39×10^{-3} (for quartzite). These values for sandstone and quartzite will be the upper and lower bounds for the simulations.

3 Results

3.1 Material behaviour for different impact velocities

First, impact simulations were conducted for steel and concrete targets (without the flight model). The vital difference between these materials is that for concrete, the dynamic penetration resistance is smaller than the dynamic penetration strength of tungsten ($R_t < Y_p$), which means that the projectile has both a rigid phase and an eroding phase, depending on the impact velocity (see Figure 5). For steel, the dynamic penetration resistance is greater than the penetration strength of tungsten ($R_t > Y_p$), meaning that the projectile only experiences eroding penetration when the impact velocity is above the critical velocity. If the impact velocity is below the critical velocity, no penetration occurs (see Figure 5).

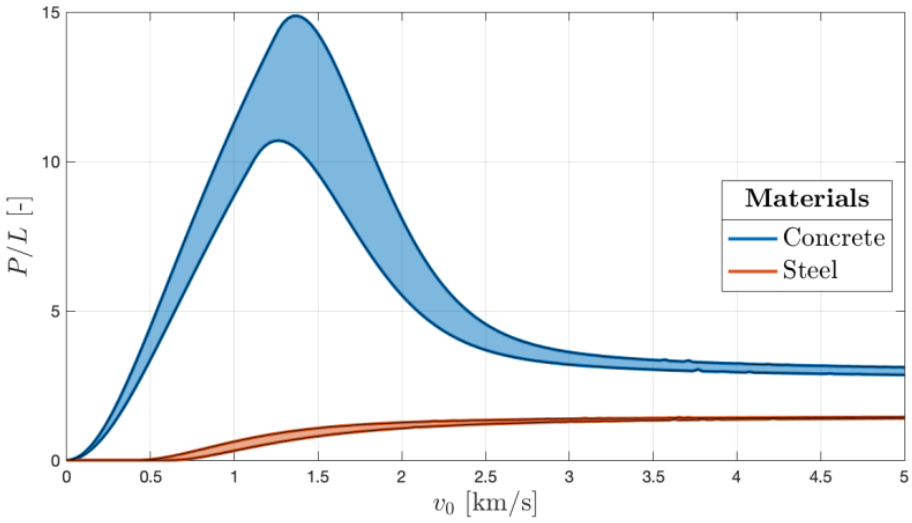

Fig. 7: Normalised penetration depth graphed for concrete (blue) and steel (orange) and for a range of impact velocities v_0.

In Figure 7, the normalised penetration depth, P/L, is calculated for a range of impact velocities v_0. The thick orange and blue lines indicate the minimum and maximum values from Table 2. What stands out in Figure 7 is that the simulated materials show very different behaviour; the graph for concrete shows an optimum while the graph for steel does not.

3.2 Orbital height

The full simulation considers the influence of the impact angles and impact velocity. Figure 8 shows the flight time of the trajectory. In this figure a significant difference can be distinguished in flight time. The higher flight altitudes result in longer flight times, obviously because the projectile travels along a longer path for a higher altitude than for lower altitude.

The resulting penetration depth is shown in Figure 9. The figure shows that the initial orbital altitude does not have a significant influence on the penetration depth. At a first glance, it may seem remarkable that for projectiles with a length of more than roughly 1 m, the penetration depth is less than the length of the projectile. However, this is a consequence of the relatively shallow impact. The orbital altitude has only a small influence on the impact parameters because the initial orbital velocity V_0 and ΔV required for deorbiting the projectile change with altitude (see Figure 10).

These impacts are shallow due to the ΔV for the projectiles in Figure 8 being calculated using a Hohmann transfer ellipse, i.e. a minimum ΔV trajectory, to a lower orbit with a perigee at an altitude of 15 km at roughly the

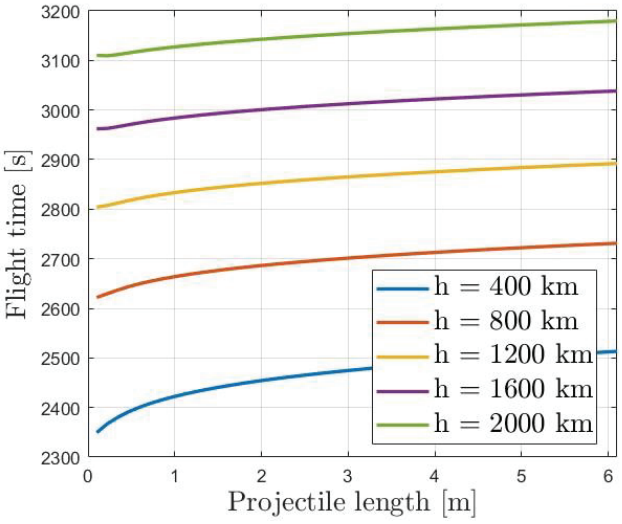

Fig. 8: Flight time as a function of the projectile length for different altitudes.

opposite side of the Earth. Below that altitude, aerodynamic drag slows the projectile down sufficiently for it to impact the ground. In Figure 11, the flight path angle (γ) for a 0.56 m projectile is shown as a function of time. This shows that for different initial orbital altitudes, the projectile enters the atmosphere at a different angle. When the projectile starts to experience aerodynamic drag, the trajectories start to look similar, resulting in roughly the same impact parameters. These trajectories are all shallow, although insufficiently shallow for ricochet to occur. In the operational context of kinetic orbital bombardment and Prompt Global Strike, a lower orbital altitude would be advisable because of the low flight time.

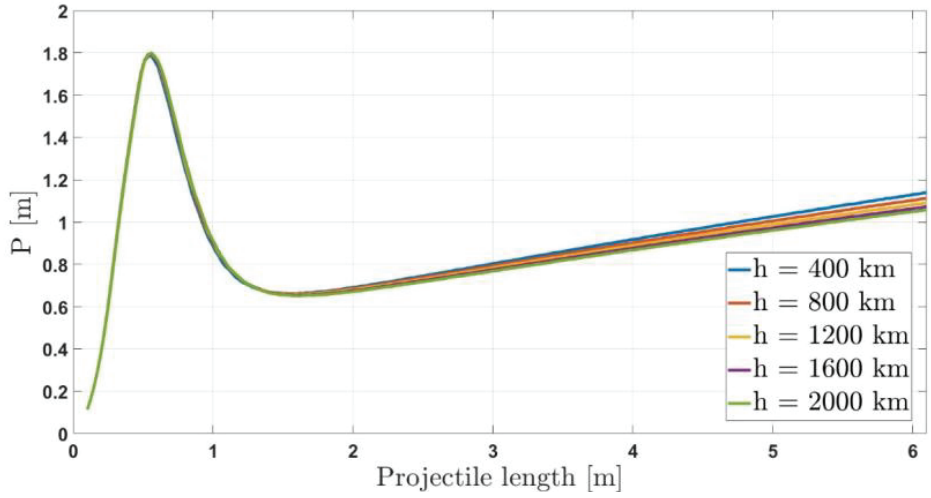

Fig. 9: Penetration depth as a function of the projectile length for concrete targets.

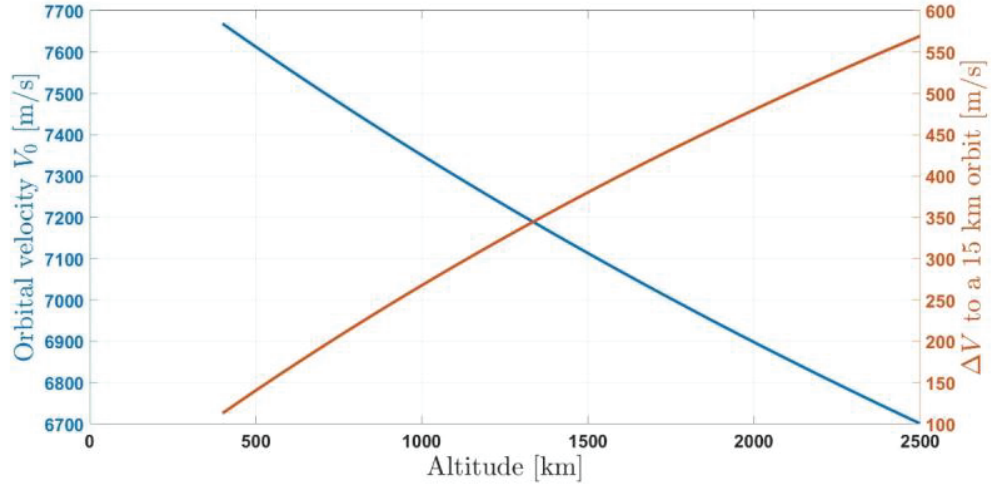

Fig. 10: Initial orbital velocity and ΔV as a function of orbital height, necessary to transfer to a 15 km orbit.

Different trajectories for deorbiting the projectiles are possible, resulting in steeper impacts, but at the cost of a higher ΔV.

3.3 Impact-induced earthquake

Earthquakes can cause significant damage to urban structures. To calculate the possible earthquake magnitudes caused by projectile impact, the magnitudes are calculated for different projectile lengths from an altitude of 400 km, using a minimal ΔV trajectory (113 m/s for $h_0 = 400$ km) for quartzite and sandstone.

Figure 12 shows a maximum magnitude of 2.5 on the Richter scale. According to the US geological survey (USGS 2010) more than 1.3 million earthquakes of this magnitude happen annually, and damage occurs above a magnitude of 4 or 5 (USGS 2022), meaning that the seismic effects caused by high velocity impacts are insignificant compared to the penetration effects.

3.4 Mass-to-orbit per projectile for different projectile lengths and launch cost estimate

The ΔV required to deorbit the projectiles significantly impacts the cost of a hypothetical orbital bombardment system. The mass-to-orbit per projectile for different values of ΔV (see Figure 10) and projectile lengths have been calculated to develop an estimate of the mass that a satellite or rocket has to carry. The mass-to-orbit is the mass of the projectile and the mass of the fuel necessary to provide a certain ΔV (see Eq. 3). Here, we neglect the mass

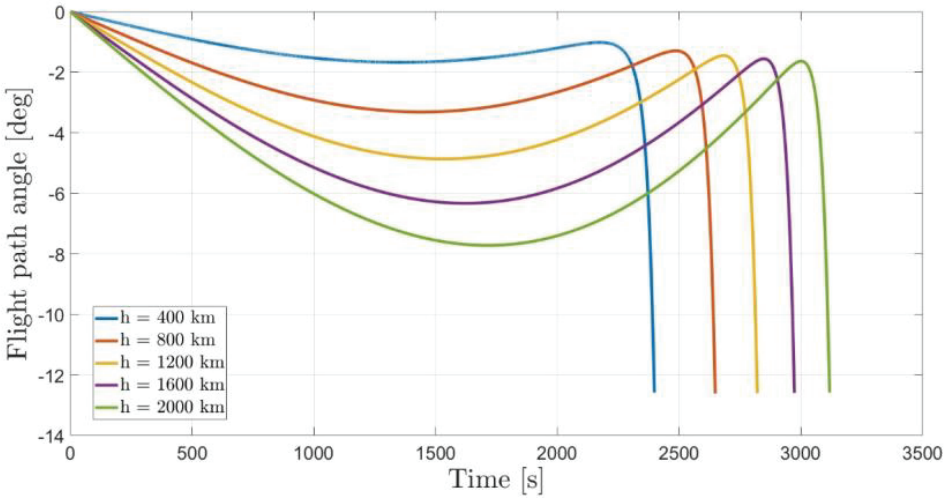

Fig. 11: Flight path angle vs. time for a projectile length of 0.56 m for different start altitudes.

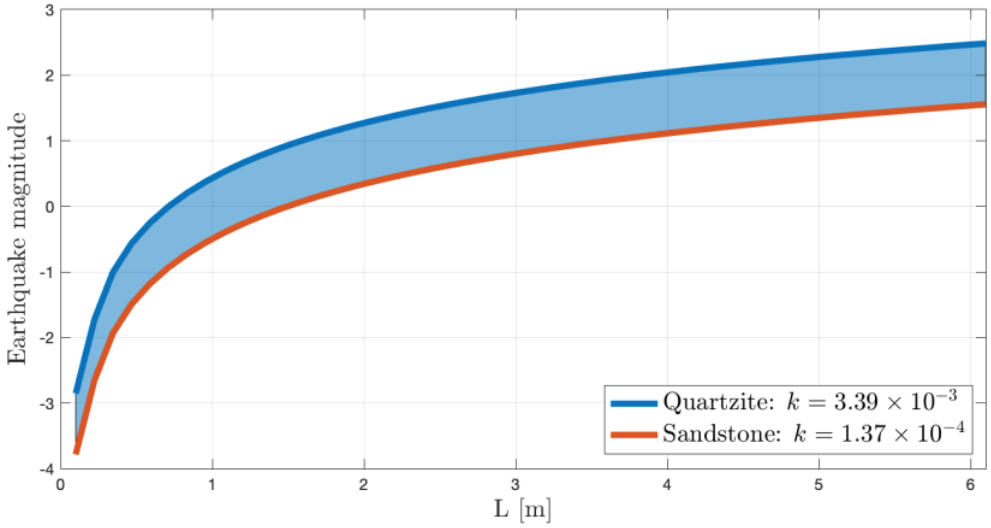

Fig. 12: Earthquake magnitude for projectile lengths ranging from 0.1 m to 6.1 m.

of the rocket motor. The ΔV ranges from the minimum ΔV (113 m/s for h_0 = 400 km) to 750 m/s and an I_{sp} = 300 s, which is a typical value for modern solid rocket motors in vacuum. These results are illustrated in Figures 13a–13c.

In spaceflight, the mass of the payload is an indication for the price to bring such a payload into an orbit. In Figure 14, the payload mass for a 4″, a 1 m and a 6.1 m projectile is presented. For a minimum ΔV, the payload masses are, respectively, 0.036 kg, 34.64 kg and 7,862 kg. For reference, the SpaceX Falcon 9 can carry a maximum payload of 22,800 kg, and has a launch costs of $56.5 million in 2013 (SpaceX 2012). This means that 1 kg payload costs roughly $2,500 to launch to a Low Earth Orbit (LEO, 400 km). For the aforementioned projectiles, this means that the launch of one projectile to LEO costs about a $100, almost a $100,000 and close to $20 million, respectively, excluding the mass of the satellite and the empty mass of the retro-rocket. The price of a system is very important, and as presented, the price increase per length is significant. Therefore, it is important to make an estimation of the influence of the length and ΔV of a projectile. Since global coverage will require multiple satellites, presumably with multiple rods, these costs soon become prohibitive.

3.5 Alternative delivery methods

There are two alternative methods to deliver a payload to its target, other than the orbital bombardment that

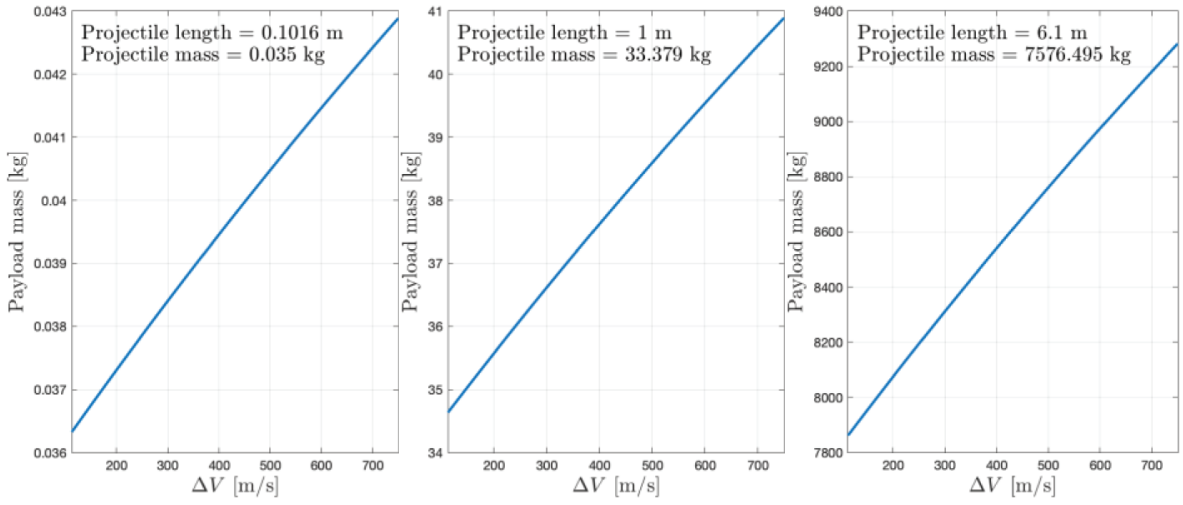

(a) Mass-to-orbit for a 4" (0.1016 m) projectile

(b) Mass-to-orbit for a 1 m projectile

(c) Mass-to-orbit for a 6.1 m projectile

Fig. 13: Mass-to-orbit per projectile for varied lengths of projectiles.

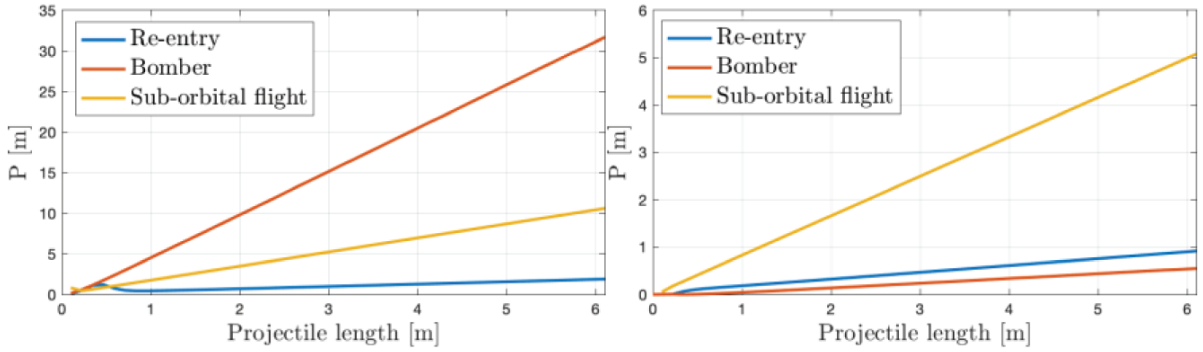

Fig. 14: Penetration depth P for concrete and steel for different methods and projectile lengths. (Left: concrete; Right: steel).

we consider in this work. It can also be dropped from a bomber or launched using an ICBM. In a comparison of the kinetic orbital bombardment system with a suborbital trajectory, the range of both trajectories has been matched. For the suborbital trajectory, we chose a burnout velocity of 6,750 m/s and a launch elevation of 30°, which are typical values for an ICBM. These parameters result in a range of approximately 6,700 km, depending on the projectile length. To match this range of the suborbital flight, the re-entry uses 435.49 m/s of ΔV and an altitude of 400 km. The simulated bomber was flying at a cruising altitude of 15 km with a cruising speed of 1,000 km/h.

For these flight trajectories, the impact velocity and impact angle can be seen in Table 3, for projectile lengths between 0.1016 m (i.e. 4″) and 6.1 m. For the impact angle, 0° is horizontal. For the impact velocity, the lower boundary corresponds to the shorter projectile and the higher boundary corresponds to the longer projectile. For the impact angle, the opposite is true.

Tab. 3: Flight parameters for different delivery methods (the range of the results is associated with the effect of the projectile length).

Method	Impact velocity [m/s]	Impact angle [°]
Re-entry	240–6,600	5–60
Bomber	250–600	63–80
Suborbital flight	1,215–6,325	35–36

The penetration depth P for concrete and steel is illustrated in Figures 14a and 14b, for concrete (left) and steel (right). For concrete targets, the bomber shows better performance for projectiles larger than 0.3 m for both the re-entry and suborbital flight. Below 0.3 m, the suborbital flight shows better performance. The better performance for the bomber is caused by the lower impact velocity since an optimum value of P/L was found for a relatively low velocity (see Figure 7) and steeper impact angle. For steel targets the suborbital methods show better performance. This is mainly caused by the higher impact velocity in combination with a high impact angle.

From these results, it is apparent that an orbital bombardment system is, in principle, less effective than using a conventional method. For steel targets, launching the projectiles with an ICBM gives a better performance and for concrete targets, using a bomber shows better performance. This is not unprecedented. The US used so-called 'Lazy Dog' kinetic projectiles dropped by aircraft in the Korean and Vietnam Wars, see e.g. Karmes (2014). More recently, in the prelude to the 2003 invasion of Iraq, the US used concrete-filled laser guided bombs, to limit collateral damage (Copp 2003a, 2003b). An obvious downside of using a bomber is that it has to fly to its destination to deliver the payload and is more susceptible to intercepts.

4 Discussion and conclusions

In the present research, projectile penetration and seismic effects of kinetic orbital bombardment systems are studied. Also, the question of whether these systems are feasible has been examined, and an analysis conducted concerning identification of the improvements that would move these systems closer to operational application.

Two different groups of materials were simulated, the first being concrete and the second being steel. Figure 7 shows that the concrete and steel targets show different behaviour. For concrete targets, an optimum impact velocity can be found, which is roughly 1400 m/s, depending on type of concrete. For steel, the optimum impact velocity is the highest achievable impact velocity because the penetration depth converges to a limit as the impact velocity increases.

The flight simulations demonstrate that changing the orbital height for a minimum ΔV trajectory does not have a significant influence on the impact angle and impact velocity. It only has an influence on the flight time and the ΔV required for the deorbit burn. In the context of kinetic orbital bombardment, the lowest sustainable orbit height would be advisable because of the low flight time (see Figure 8).

Combining the impact simulation and the re-entry simulations shows that a bottleneck of this concept is the impact angle (γ) of the projectile. Unfortunately, a higher impact velocity is not better because it also implies a smaller impact angle. Without adjustments, the concept is not feasible. For concrete targets, the most sensible result is a projectile length of 0.56 m, penetrating 1.79 m, with a minimal ΔV trajectory. This projectile is the most plausible because the same performance can be achieved with larger projectiles but at a significantly increased price.

The shallow angle is a result of the choice of using a Hohmann transfer to 15 km. At this height the projectile will be captured by the atmosphere. Applying a much larger ΔV would result in a suborbital trajectory and a steeper descent, but also result in a smaller impact velocity and at the expense of a significantly larger launch mass. For an orbital altitude of 400 km, the best performance is achieved when the largest projectile (L = 8 m) comes to a complete standstill from its orbital velocity ($\Delta V = V_{\text{orbit}}$ = 7667 m/s) and descends in a vertical line towards the Earth. For concrete a penetration depth of 32 m is achieved and for steel a penetration depth of 11 m is achieved. However, an 8 m projectile with a ΔV of 7,667 m/s requires a total payload mass of at least 32,919 kg. Such a payload would cost at least $82 million to launch to LEO. These high costs make the concept less feasible.

The calculations show that the impact of a tungsten alloy rod with a length of 8 m and a 0.4 m diameter results in an earthquake with a seismic magnitude of only 2.5 on the Richter scale. Approximately 1.3 million of such earthquakes happen every year, indicating that the seismic effect is insignificant. An earthquake with a magnitude of 2.5 is generally not felt and only recorded by seismic centres. This clearly shows that kinetic bombardment is not a WMD.

Moreover, alternative delivery methods show better performance for both steel and concrete targets. If a bomber would drop the same projectile from 15 km altitude, the projectile would penetrate 2.5 m. For steel targets, a 1 m projectile would penetrate 0.2 m, and using an ICBM, the same projectile would penetrate 1 m. Both these are methods in relation to which a significant amount of experience has already been accumulated, and it is thus apparent that a kinetic orbital bombardment system cannot be considered a serious alternative. The flight time might appear to be a clear advantage. A bomber would need to fly to its targets, be vulnerable and deliver the payload. An ICBM has a flight time of roughly 30 min, whereas an orbital bombardment system has a flight time ranging from 5 min to 15 min. However, this is solely the flight time of the projectile, and thus excluding the time required for an orbital bombardment satellite to fly or manoeuvre to suitable initial conditions for launching the projectile.

Two adjustments would make the concept more feasible. The first adjustment is to use a hypersonic drag device to decelerate the projectile. Even though this reduces the impact velocity, it results in better penetration performance because the impact angle is steeper. Depending on the ability to increase the drag, the penetration depth can be increased. If the drag can be increased by a factor 10,

the best penetration would be provided by a tungsten projectile with a length of 5 m and a diameter of 0.25 m, with a penetration depth of 18 m. The second adjustment is to accept a very high price. By doing so, heavy projectiles with a significant amount of propellant can be brought into orbit, resulting in a large ΔV and a large projectile length. For concrete, an 8 m tungsten projectile with a diameter of 0.4 m would penetrate roughly 30 m and for steel roughly 10 m. Future work on this concept could also include optimising the impact effect as a function of the projectile mass and the ΔV required for deorbiting trajectories that provide steeper impact angles.

Further important topics for operational application that were not explicitly included in this study are the accuracy of the weapon system and the number of satellites necessary to be able to cover the entirety of the Earth's surface. Since the projectile itself is unable to manoeuvre, it would be difficult to accurately hit a target. This also applies to re-entry vehicles of ICBMs, but they typically carry nuclear warheads, such that accuracy is less important. Since the damage of a kinetic orbital bombardment system is essentially caused by penetration, the damage radius of the projectile is very small. It is therefore crucial that the system be very accurate. This requires some form of guidance and flight control, and it may not be possible to achieve this at the relevant velocities. Conventionally armed ballistic missiles, with a considerably smaller damage radius than that of a nuclear warhead, have a similar issue. Some do have guided re-entry vehicles with fins for flight control, to improve their accuracy, but these operate at much smaller velocities. The other topic is, as mentioned, the number of satellites needed to achieve an adequate coverage of the Earth's surface. The weapon system should be able to strike any place on Earth in a short time. For this purpose, a large constellation of satellites is necessary. Furthermore, to ensure a short response time, the vehicle that deorbits the rod should also carry propellant for out-of-plane manoeuvres, as well as for a larger ΔV than is required for the rod's orbit to have a perigee at 15 km above the Earth on the other side of the planet. If it does not, it would take a long time for the impact point of a projectile launched by any of the satellites to coincide with a given target position on the Earth's surface. Obviously, this propellant adds even more to the launch mass.

Little quantitative information about the different kinetic orbital bombardment systems that have been considered is available and we have used simplified models. For instance, the ΔV for the transfer to a lower altitude was approximated as instantaneous and we have used a one-dimensional model for the projectile impact. We have also not used different projectile shapes. However, our results clearly show some of the inherent limitations of such a system and these would not change significantly if we were to use somewhat different numbers for the parameters or more detailed physics models. To summarise, orbital bombardment systems are not feasible, unless adjustments are made to provide the required impact angle and sufficient accuracy can be achieved. At present, alternative methods such as long rods being dropped by a bomber or launched by an ICBM seem more feasible.

References

Alekseevskii, V. P. (1966). Penetration of a rod into a target at high velocity. *Combustion, Explosion, and Shock Waves, 2*(2), pp. 63-66.

Anderson, J. D. (2016). *Introduction to Flight,* 8th edn. McGraw-Hill, New York.

Bavdekar, S., Parsard, G., Subhash, G., & Satapathy, S. (2017). An improved dynamic expanding cavity model for high-pressure and high-strain rate response of ceramics. *International Journal of Solids and Structures, 125*(77), p. 88. doi: 10.1016/j.ijsolstr.2017.07.014.

Bavdekar, S., Subhash, G., & Satapathy, S. (2019). A unified model for dwell and penetration during long rod impact on thick ceramic targets. *International Journal of Impact Engineering, 131*(May), pp. 304-316. doi: 10.1016/j.ijimpeng.2019.05.014.

Bear, G. (2005). *Quantico*. HarperCollins Publishers, London.

Bond, J. W. (1958). Plasma physics and hypersonic flight. *Journal of Jet Propulsion, 28*, pp. 228-235. doi: 10.2514/8.7284.

Braun, W. F. (1973). Aerodynamic data for small arms projectiles. US Ballistic Research Laboratories, Aberdeen Proving Ground, Maryland.

Butler, D. K. Nielsen, R. R., Dropek, R. K., & Butters, S. W. (1977). Constitutive Property Investigations in Support of Full-Scale Penetration Tests in Dakota Sandstone, San Ysidro, New Mexico, Technical Report S-77-3, Washington, DC.

Chapman, S., & Cowling, T. G. (1970). The Mathematical Theory of Non-uniform Gases: An Account of the Kinetic Theory of Viscosity, Thermal Conduction and Diffusion in Gases. Cambridge University Press, Cambridge.

Copp, K. (2003a). Iraqi freedom – guided munitions. *Australian Aviation*, (June), pp. 1-6.

Copp, K. (2003b). The Hammer & Anvil. *Australian Aviation*, (May), pp. 25-35.

Curtis, H. (2005). *Orbital Mechanics for Engineering Students*. Elsevier, Amsterdam.

Elbasheer, R. M. (2014). K-BOMB: Analysis of G/LEO Kinetic Bombardment and Application to National Security Strategies for Full-Spectrum Military Interoperability, A002-R02-2014, Project Polemos.

Flis, W. J. (2016). Modified Alekseevskii–Tate model for rod penetration of porous targets. *Proceedings - 29th International Symposium on Ballistics, 2*(2), pp. 2219-2227.

Frew, D. J., Hanchak, S. J., Green, M.L., & Forrestal, M.J. (1998). Penetration of concrete targets with ogive-nose steel rods. *International Journal of Impact Engineering, 21*(6), pp. 489-497. doi: 10.1016/S0734-743X(98)00008-6.

Güldemeister, N., & Wünnemann, K. (2017). Quantitative analysis of impact-induced seismic signals by numerical modeling. *Icarus, 296*, pp. 15-27. doi: 10.1016/j.icarus.2017.05.010.

Gutenberg, B., & Richter, C. F. (1955). Magnitute and energy of earthquakes. *Nature, 176*(4486), p. 795.

Hankey, W. L. (1988). *Re-Entry Aerodynamics*. AIAA, Washington, DC.

Hibbeler, R. C. (2020). *Fluid Mechanics*. Pearson, London.

Hohler, V., & Stilp, A. J. (1990). Long-rod penetration mechanics. In: Zukas, J. A. (ed.), *High Velocity Impact Dynamics*. John Wiley & Sons, New York, pp. 321-404.

Holmquist, T. J., Johnson, G. R., & Cook, W. H. (1993). Computational constitutive model for concrete subjected to large strains, high strain rates, and high pressure. In: *14th International Symposium on Ballistics*, pp. 591-600.

Johnson-Freese, J. (2017). Space Warfare in the 21st Century: Arming the Heavens. Routledge, London and New York.

Karmes, D. (2014). The Patricia Lynn Project: Vietnam War, the Early Years of Air Intelligence. iUniverse, Bloomington, IN.

Larson, C. (2020). *'Rods from God': Why Mach 5 Hypersonic Tugeston Bombs Were Never Dropped, 16 November*, *National Interest*. Available at: https://nationalinterest.org/blog/buzz/rods-god-why-mach-5-hypersonic-tugeston-bombs-were-never-dropped-172663 [accessed 22 November 2022].

Noble, C., Kokko, E., Darnell, I., Dunn, T., Hagler, L., & Leininger, L. (2005). Concrete Model Descriptions and Summary of Benchmark Studies for Blast Effects Simulations. University of California, Lawrence Livermore National Laboratory.

Pournelle, J. P. (1974). A step farther out: Halfway to anywhere. *Galaxy, 34*(7), pp. 94-101.

SpaceX (2012). *Capabilities and services*, [Online]. Available at: https://web.archive.org/web/20131005123104/http://www.spacex.com/about/capabilities.

Stilwell, B. (2020). *These Air Force 'rods from God' could hit with the force of a nuclear weapon, 10 September*, *We are the mighty*. Available at: https://www.wearethemighty.com/articles/these-air-force-rods-from-god-could-hit-with-the-force-of-a-nuclear-weapon/ [accessed 22 November, 2022].

Stokes, E., Yarrington, P., & Glenn, L. (2005) *An Earth Penetrating Modeling Assessment, UCRL-TR-213206*. doi: 10.2172/919237.

Tate, A. (1969). Further results in the theory of long rod penetration. *Journal of the Mechanics and Physics of Solids, 17*(3), pp. 141-150. doi: 10.1016/0022-5096(69)90028-3.

Tate, A. (1979). A simple estimate of the minimum target obliquity required for the ricochet of a high speed long rod projectile. *Journal of Physics D: Applied Physics, 12*(11), pp. 1825-1829. doi: 10.1088/0022-3727/12/11/011.

Tate, A. (1986). Long rod penetration models – Part II. Extensions to the hydrodynamic theory of penetration. *International Journal of Mechanical Sciences, 28*(9), pp. 599-612. doi: 10.1016/0020-7403(86)90075-5.

UN Outer Space Treaty of 1966. Article IV (1966). https://www.unoosa.org/oosa/en/ourwork/spacelaw/treaties/outerspacetreaty.html

USGS (2010). *Earthquake Facts and Statistics*, *US Geological Survey*. Available at: https://www.unoosa.org/oosa/en/ourwork/spacelaw/treaties/outerspacetreaty.html.

USGS (2022). *At what magnitude does damage begin to occur in an earthquake? US Geological Survey*. Available at: https://www.usgs.gov/faqs/what-magnitude-does-damage-begin-occur-earthquake.

Vahedi, K., Latifi, M., & Khosravi, F. (2008). Investigation and analysis of ogive-shape nose steel projectile into concrete target. *Turkish Journal of Engineering and Environmental Sciences, 32*(5), pp. 295-302.

Walker, J. D. (2021). *Modern Impact and Penetration Mechanics,* 1st edn. Cambridge University Press, Cambridge, UK. doi: 10.1017/9781108684026.

Warren, T. L., Hanchak, S. J., & Poormon, K. L. (2004). Penetration of limestone targets by ogive-nosed VAR 4340 steel projectiles at oblique angles: Experiments and simulations. *International Journal of Impact Engineering, 30*(10), pp. 1307-1331. doi: 10.1016/j.ijimpeng.2003.09.047.

Watts, B. D. (2005). Long-Range Strike: Imperatives, Urgency and Options. Center for Strategic and Budgetary Assessments, Washington, DC.

Wiesel, W. E. (2010). *Spaceflight Dynamics*, 3rd edn. Aphelion Press, Beavercreek, OH.

Zheng, L., Yuanxue, L., Ming, H., & Wu, R. (2016). Evaluation of damage effect of God stick space-based kinetic energy weapon (in Chinese). *Journal of vibration and shock, 35*(18), pp. 159-165.